# New Power Source from Fractional Quantum Energy Levels of Atomic Hydrogen that Surpasses Internal Combustion

**Randell L. Mills, Paresh Ray, Bala Dhandapani, Mark Nansteel, Xuemin Chen, Jiliang He**

BlackLight Power, Inc.

493 Old Trenton Road

Cranbury, NJ 08512

(609) 490-1090

(609) 490-1066 FAX

## ABSTRACT

Extreme ultraviolet (EUV) spectroscopy was recorded on microwave discharges of helium with 2% hydrogen. Novel emission lines were observed with energies of $q \cdot 13.6\ eV$ where $q = 1,2,3,4,6,7,8,9,$ *or* $11$ or these lines inelastically scattered by helium atoms wherein $21.2\ eV$ was absorbed in the excitation of $He(1s^2)$ to $He(1s^1 2p^1)$. These lines were identified as hydrogen transitions to electronic energy levels below the "ground" state corresponding to fractional quantum numbers. Significant line broadening corresponding to an average hydrogen atom temperature of 33 - 38 $eV$ was observed for helium-hydrogen discharge plasmas; whereas, pure hydrogen showed no excessive broadening corresponding to an average hydrogen atom temperature of $\approx 3\ eV$. Since a significant increase in ion temperature was observed with helium-hydrogen discharge plasmas, and energetic hydrino lines were observed at short wavelengths in the corresponding microwave plasmas that required a very significant reaction rate due to low photon detection efficiency in this region, the power balance was measured on the helium-hydrogen microwave plasmas. With a microwave input power of 30 $W$, the thermal output power was measured to be at least 300 $W$ corresponding to a reactor temperature rise from room temperature to 900 °C within 90 seconds, a power density of 30 $MW/m^3$, and an energy balance of about $-4\ X10^5\ kJ/mole\ H_2$ compared to the enthalpy of combustion of hydrogen of $-241.8\ kJ/mole\ H_2$.

# I. INTRODUCTION

From a solution of a Schrödinger-type wave equation with a nonradiative boundary condition based on Maxwell's equations, Mills predicts that atomic hydrogen may undergo a catalytic reaction with certain atomized elements and ions which singly or multiply ionize at integer multiples of the potential energy of atomic hydrogen, $m \cdot 27.2\ eV$ wherein $m$ is an integer [1, 6-28]. The reaction involves a nonradiative energy transfer to form a hydrogen atom that is lower in energy than unreacted atomic hydrogen that corresponds to a fractional principal quantum number ($n = \frac{1}{p} = \frac{1}{\text{integer}}$ replaces the well known parameter $n = \text{integer}$ in the Rydberg equation for hydrogen excited states). One such atomic catalytic system involves helium ions because the second ionization energy of helium is $54.417\ eV$, which is equivalent to $m = 2$. In this case, the catalysis reaction is

$$54.417\ eV + He^+ + H[a_H] \rightarrow He^{2+} + e^- + H\left[\frac{a_H}{3}\right] + 108.8\ eV \quad (1)$$

$$He^{2+} + e^- \rightarrow He^+ + 54.417\ eV \quad (2)$$

And, the overall reaction is

$$H[a_H] \rightarrow H\left[\frac{a_H}{3}\right] + 54.4\ eV + 54.4\ eV \quad (3)$$

Since the products of the catalysis reaction have binding energies of $m \cdot 27.2\ eV$, they may further serve as catalysts. Thus, further catalytic transitions may occur: $n = \frac{1}{3} \rightarrow \frac{1}{4}$, $\frac{1}{4} \rightarrow \frac{1}{5}$, and so on. In this process called *disproportionation*, lower-energy hydrogen atoms, *hydrinos*, can act as catalysts because each of the metastable excitation, resonance excitation, and ionization energy of a hydrino atom is $m \cdot 27.2\ eV$. The transition reaction mechanism of a first hydrino atom affected by a second hydrino atom involves the resonant coupling between the atoms of $m$ degenerate multipoles each having $27.21\ eV$ of potential energy [1, 6-28]. The energy transfer of $m \cdot 27.2\ eV$ from the first hydrino atom to the second hydrino atom causes the central field of the first atom to increase by $m$ and its electron to drop $m$ levels lower from a radius of $\frac{a_H}{p}$ to a radius of $\frac{a_H}{p+m}$. The second interacting lower-energy hydrogen is either excited to a

metastable state, excited to a resonance state, or ionized by the resonant energy transfer.

The resonant transfer may occur in multiple stages. For example, a nonradiative transfer by multipole coupling may occur wherein the central field of the first increases by $m$, then the electron of the first drops $m$ levels lower from a radius of $\frac{a_H}{p}$ to a radius of $\frac{a_H}{p+m}$ with further resonant energy transfer. The energy transferred by multipole coupling may occur by a mechanism that is analogous to photon absorption involving an excitation to a virtual level. Or, the energy transferred by multipole coupling during the electron transition of the first hydrino atom may occur by a mechanism that is analogous to two photon absorption involving a first excitation to a virtual level and a second excitation to a resonant or continuum level [29-31]. The transition energy greater than the energy transferred to the second hydrino atom may appear as a photon in a vacuum medium.

The transition of $H\left[\frac{a_H}{p}\right]$ to $H\left[\frac{a_H}{p+m}\right]$ induced by a multipole resonance transfer of $m \cdot 27.21\,eV$ and a transfer of $[(p')^2-(p'-m')^2]\,X\,13.6\,eV - m \cdot 27.2\,eV$ with a resonance state of $H\left[\frac{a_H}{p'-m'}\right]$ excited in $H\left[\frac{a_H}{p'}\right]$ is represented by

$$H\left[\frac{a_H}{p'}\right]+H\left[\frac{a_H}{p}\right]\rightarrow H\left[\frac{a_H}{p'-m'}\right]+H\left[\frac{a_H}{p+m}\right]+[\left((p+m)^2-p^2\right)-\left(p'^2-(p'-m')^2\right)]\,X\,13.6\,eV \quad (4)$$

where $p$, $p'$, $m$, and $m'$ are integers.

Hydrinos may be ionized during a disproportionation reaction by the resonant energy transfer. A hydrino atom with the initial lower-energy state quantum number $p$ and radius $\frac{a_H}{p}$ may undergo a transition to the state with lower-energy state quantum number $(p+m)$ and radius $\frac{a_H}{(p+m)}$ by reaction with a hydrino atom with the initial lower-energy state quantum number $m'$, initial radius $\frac{a_H}{m'}$, and final radius $a_H$ that provides a net enthalpy of $m \cdot 27.2\,eV$. Thus, reaction of hydrogen-type

atom, $H\left[\frac{a_H}{p}\right]$, with the hydrogen-type atom, $H\left[\frac{a_H}{m'}\right]$, that is ionized by the resonant energy transfer to cause a transition reaction is represented by

$$m\,X\,27.21\,eV + H\left[\frac{a_H}{m'}\right] + H\left[\frac{a_H}{p}\right] \rightarrow H^+ + e^- + H\left[\frac{a_H}{(p+m)}\right] + [(p+m)^2 - p^2 - (m'^2 - 2m)]X13.6\,eV \quad (5)$$

$$H^+ + e^- \rightarrow H\left[\frac{a_H}{1}\right] + 13.6\,eV \quad (6)$$

And, the overall reaction is

$$H\left[\frac{a_H}{m'}\right] + H\left[\frac{a_H}{p}\right] \rightarrow H\left[\frac{a_H}{1}\right] + H\left[\frac{a_H}{(p+m)}\right] + [2pm + m^2 - m'^2]X13.6\,eV + 13.6\,eV \quad (7)$$

It is further proposed that the photons that arise from hydrogen catalysis may undergo inelastic helium scattering. That is, the catalytic reaction

$$H[a_H] \xrightarrow{He^*} H\left[\frac{a_H}{3}\right] + 54.4\,eV + 54.4\,eV \quad (8)$$

yields two $54.4\,eV$ photons ($22.8\,nm$). When each of these photons strikes $He\,(1s^2)$, $21.2\,eV$ is absorbed in the excitation to $He\,(1s^1 2p^1)$. This leaves a $33.19\,eV$ ($37.4\,nm$) photon peak shown in Table 1. Thus, for helium the inelastic scattered peak of $54.4\,eV$ photons from Eq. (3) is given by

$$E = 54.4\,eV - 21.21\,eV = 33.19\,eV\ (37.4\,nm) \quad (9)$$

The general reaction is

$$photon\,(h\nu) + He\,(1s^2) \rightarrow He\,(1s^1 2p^1) + photon\,(h\nu - 21.21\,eV) \quad (10)$$

A number of independent experimental observations lead to the conclusion that atomic hydrogen can exist in fractional quantum states that are at lower energies than the traditional "ground" ($n=1$) state. Prior related studies that support the possibility of a novel reaction of atomic hydrogen which produces a chemically generated or assisted plasma and produces novel hydride compounds include extreme ultraviolet (EUV) spectroscopy [7-12, 15-19], characteristic emission from catalysis and the hydride ion products [9-10], lower-energy hydrogen emission [5, 7-8], plasma formation [9-12, 15-16, 18-19], Balmer $\alpha$ line broadening [13], anomalous plasma afterglow duration [18-19], power generation [11-15, 26], and analysis of chemical compounds [20-26]. We report that microwave and glow discharges of helium-hydrogen mixtures were studied by extreme ultraviolet (EUV) spectroscopy to search for hydrino

lines. Since the corresponding electronic transitions are very energetic, Balmer $\alpha$ line broadening was anticipated and was measured. Since the second ionization energy of $He^+$ is an exact multiple of the potential energy of atomic hydrogen and microwave plasmas may have significant concentrations of $He^+$ as well as atomic hydrogen, fast kinetics observable as heat may be possible. Thus, power balances of microwave plasmas of helium-hydrogen mixtures were also measured.

## II. EXPERIMENTAL

### A. EUV Spectroscopy

EUV spectroscopy was recorded on hydrogen, helium, and helium-hydrogen (98/2%) microwave and glow discharge plasmas according to the methods given previously [7]. The glow discharge experimental set up was given previously [7]. The microwave experimental set up comprising a microwave discharge gas cell light source and an EUV spectrometer which was differentially pumped is shown in Figure 1. Helium-hydrogen (98/2%) gas mixture was flowed through a half inch diameter quartz tube at 1 torr, 20 torr, or 760 torr. The gas pressure inside the cell was maintained by flowing the mixture while monitoring the pressure with a 10 torr and 1000 torr MKS Baratron absolute pressure gauge. By the same method, the hydrogen alone and helium alone plasmas were run at 20 torr. The tube was fitted with an Opthos coaxial microwave cavity (Evenson cavity). The microwave generator was a Opthos model MPG-4M generator (Frequency: 2450 MHz). The input power to the plasma was set at 85 watts with air cooling of the cell.

The spectrometer was a normal incidence McPherson 0.2 meter monochromator (Model 302, Seya-Namioka type) equipped with a 1200 lines/mm holographic grating with a platinum coating. The wavelength region covered by the monochromator was $5-560\,nm$. The EUV spectrum was recorded with a channel electron multiplier (CEM) at $2500-3000\,V$. The wavelength resolution was about $0.02\,nm$ (FWHM) with an entrance and exit slit width of $50\,\mu m$. The increment was $0.2\,nm$ and the dwell time was $500\,ms$. Novel peak positions were based on a calibration against the known He I and He II lines.

To achieve higher sensitivity at the shorter EUV wavelengths, the light emission from a helium microwave plasma and a glow discharge plasma of a helium-hydrogen mixture (98/2%) maintained according to the methods given previously [7] were recorded with a McPherson 4° grazing incidence EUV spectrometer (Model 248/310G) equipped with a grating having 600 G/mm with a radius of curvature of $\approx 1\,m$. The angle of incidence was 87°. The wavelength region covered by the monochromator was $5-65\,nm$. The wavelength resolution was about $0.04\,nm$ (FWHM) with an entrance and exit slit width of $300\,\mu m$. A channel electron multiplier (CEM) at $2400\,V$ was used to detect the EUV light. The increment was $0.1\,nm$ and the dwell time was $1\,s$.

## B. Line broadening measurements

The width of the 656.2 nm Balmer $\alpha$ line emitted from gas glow discharge plasmas having atomized hydrogen from pure hydrogen alone or with a mixture of 10% hydrogen and helium at 2 torr total pressure was measured according to the methods given previously [11]. The plasmas were maintained in a cylindrical stainless steel gas cell (9.21 cm in diameter and 14.5 cm in height) with an axial hollow cathode glow discharge electrode assembly comprised a stainless steel plate (4.2 cm diameter, 0.9 mm thick) anode and a circumferential stainless steel cylindrical frame (5.1 cm OD, 7.2 cm long) perforated with evenly spaced 1 cm diameter holes. The emission was viewed normal to the cell axis through a 1.6 mm thick UV-grade sapphire window with a 1.5 cm view diameter. The discharge was carried out under static gas conditions with a DC voltage of about 275 V which produced about 0.2 A of current. The plasma emission from the glow discharges was fiber-optically coupled through a 220F matching fiber adapter to a high resolution visible spectrometer with a resolution of $\pm 0.025\,nm$ over the spectral range $190-860\,nm$. The entrance and exit slits were set to $20\,\mu m$. The spectrometer was scanned between $656-657\,nm$ using a $0.01\,nm$ step size. The signal was recorded by a PMT with a stand alone high voltage power supply (950 V) and an acquisition controller. The data was obtained in a single accumulation with a 1 second integration time.

### C. Power balance measurements

The power balances of microwave plasmas of helium, krypton, and xenon alone and each noble gas with 10% hydrogen were determined by heat loss calorimetry [32] in the cell described in section A except that the cell was not air cooled. A K-type thermocouple ($\pm 0.1\ ^{\circ}C$) housed in a stainless steel tube was placed axially inside the center of the 10 $cm^3$ plasma volume of the quartz microwave cell. The thermocouple was read with a multichannel computer data acquisition system. The gas in each case was ultrahigh purity grade or higher. The gas pressure inside the cell was maintained at about 300 mtorr with a noble gas flow rate of 9.3 sccm or an noble gas flow rate of 8.3 sccm and a hydrogen flow rate of 1 sccm. Each gas flow was controlled by a 0-20 sccm range mass flow controller (MKS 1179A21CS1BB) with a readout (MKS type 246). The cell pressure was monitored by a 0-10 torr MKS Baratron absolute pressure gauge.

No increase in temperature was observed when 10% hydrogen was added to krypton or xenon plasmas. In contrast, with the addition of 10% hydrogen to a helium plasma, the quartz wall was observed to melt in about 90 seconds unless the power was 30 W or less. Whereas, the helium alone plasma at 60 W input had a maximum temperature rise above room temperature, $\Delta T$, of 178 °C at 90 seconds. Thus, to achieve a higher control $\Delta T$ to give greater analytical accuracy, the temperature rise of the inside of the cell was measured for 90 seconds with helium at 60 W input. The input power was stopped, and a cooling curve was measured. Then the experiment was repeated with the addition of 10% hydrogen to the helium run at only 30 W to prevent the cell from melting. In additional controls, noncatalysts krypton or xenon replaced helium.

## III. RESULTS AND DISCUSSION

### A. EUV Spectroscopy

The EUV emission was recorded from microwave and glow discharge plasmas of hydrogen, helium, and helium with 2% hydrogen

over the wavelength range 5-125 *nm*. In the case of hydrogen, no peaks were observed below 78 *nm*, and no spurious peaks or artifacts due to the grating or the spectrometer were observed. Only known He I and He II peaks were observed in the EUV spectra of the control helium microwave or glow discharge cell emission.

The EUV spectra (15 – 50 *nm*) of the microwave cell emission of the helium-hydrogen mixture (98/2%) that was recorded at 1, 24, and 72 hours and the helium control (dotted curve) is shown in Figure 2. Ordinary hydrogen has no emission in these regions. Peaks observed at 45.6 *nm*, 37.4 *nm*, and 20.5 *nm* which do not correspond to helium and increased with time were assigned to lower-energy hydrogen transitions in Table 1. The lines that corresponded to hydrogen transitions to lower electronic energy levels were not observed in the helium control. The pressure was increased from 20 torr to 760 torr. The peaks appeared slightly more intense at the lower pressure; so, the pressure was decreased to 1 torr and spectra were recorded.

At the 1 torr condition, additional novel peaks were observed in the short wavelength region. The short wavelength EUV spectrum (5 – 50 *nm*) of the control hydrogen microwave cell emission (bottom curve) is shown in Figure 3. No spectrometer artifacts were observed at the short wavelengths. The short wavelength EUV spectrum (5 – 50 *nm*) of the helium-hydrogen mixture (98/2%) microwave cell emission with a pressure of 1 torr (top curve) is also shown in Figure 3. Peaks observed at 14.15 *nm*, 13.03 *nm*, 10.13 *nm*, and 8.29 *nm* which do not correspond to helium were assigned to lower-energy hydrogen transitions in Table 1. It is also proposed that the 30.4 *nm* peak shown in Figures 2 and 3 was not entirely due to the He II transition. In the case of helium-hydrogen mixture, conspicuously absent was the 25.6 *nm* (48.3 *eV*) line of He II shown in Figure 2 which implies only a minor He II transition contribution to the 30.4 *nm* peak.

A novel 63.3 *nm* peak was observed in the EUV spectrum (50 – 65 *nm*) of the helium-hydrogen mixture (98/2%) glow discharge cell emission shown in Figure 4. It is proposed that the 63.3 *nm* peak arises from inelastic helium scattering of the 30.4 *nm* peak. That is, the $\frac{1}{3} \rightarrow \frac{1}{4}$ transition yields a 40.8 *eV* photon (30.4 *nm*). When this photon strikes

$He(1s^2)$, $21.2\,eV$ is absorbed in the excitation to $He(1s^1 2p^1)$. This leaves a $19.6\,eV$ ($63.3\,nm$) photon and a $21.2\,eV$ ($58.4\,nm$) photon from $He(1s^1 2p^1)$. The intensity of the $58.4\,nm$ shown in Figure 4 was off-scale with 56,771 photons/sec. Thus, the transition $He(1s^2) \rightarrow He(1s^1 2p^1)$ dominated the inelastic scattering of EUV peaks. For the first nine peaks assigned as lower-energy hydrogen transitions or such transitions inelastically scattered by helium, the agreement between the predicted values and the experimental values shown in Table 1 is remarkable. It is also remarkable that the hydrino lines are moderately intense based on the low grating efficiency at these short wavelengths.

As shown in Figures 5 and 6, the ratio of the L$\beta$ peak to the $91.2\,nm$ peak of the helium-hydrogen microwave plasma was 2; whereas, the ratio of the L$\beta$ peak to the $91.2\,nm$ peak of the control hydrogen microwave plasma was 8 which indicates that the majority of the $91.2\,nm$ peak was due to a transition other than the binding of an electron by a proton. Based on the intensity, it is proposed that the majority of the $91.2\,nm$ peak was due to the $\frac{1}{2} \rightarrow \frac{1}{4}$ transition given in Table 1.

The energies for the hydrogen transitions given in Table 1 in order of energy are $13.6\,eV$, $27.2\,eV$, $40.8\,eV$, $54.4\,eV$, $81.6\,eV$, $95.2\,eV$, $108.8\,eV$, $122.4\,eV$ and $149.6\,eV$. The corresponding peaks are $91.2\,nm$, $45.6\,nm$, $30.4\,nm$ with $63.3\,nm$, $37.4\,nm$, $20.5\,nm$, $13.03\,nm$, $14.15\,nm$, $10.13\,nm$, and $8.29\,nm$, respectively. Thus, the lines identified as hydrogen transitions to electronic energy levels below the "ground" state corresponding to fractional quantum numbers correspond to energies of $q \cdot 13.6\,eV$ where $q = 1,2,3,4,6,7,8,9,$ *or* $11$ or these lines inelastically scattered by helium atoms wherein $21.2\,eV$ was absorbed in the excitation of $He(1s^2)$ to $He(1s^1 2p^1)$. All other peaks besides those assigned to lower-energy hydrogen transitions could be assigned to He I, He II, second order lines, or atomic or molecular hydrogen emission. No known lines of helium or hydrogen explain the $q \cdot 13.6\,eV$ related set of peaks. Given that these spectra are readily repeatable, these peaks may have been overlooked in the past without considering the role of the helium scattering.

### B. Line broadening measurements

The results of the 656.2 nm Balmer $\alpha$ line width measured with a high resolution ($\pm 0.025\,nm$) visible spectrometer on glow discharge plasmas having atomized hydrogen from pure hydrogen alone and helium-hydrogen (90/10%) is given in Figure 7. Using the method of Kuraica and Konjevic [33] and Videnocic et al. [34], the energetic hydrogen atom densities and energies were calculated. It was found that helium-hydrogen showed significant broadening corresponding to an average hydrogen atom temperature of $33\text{-}38\,eV$ and an atom density of $3 X 10^{13}\,atoms/cm^3$; whereas, pure hydrogen showed no excessive broadening corresponding to an average hydrogen atom temperature of $\approx 3\,eV$ and an atom density of only $5 X 10^{13}\,atoms/cm^3$ ever though 10 times more hydrogen was present.

## C. Power balance measurements

Since a significant increase in ion temperature was observed with helium-hydrogen discharge plasmas, and energetic hydrino lines were observed at short wavelengths in the corresponding microwave plasmas that required a very significant reaction rate due to low photon detection efficiency in this region, the power balance was measured on the helium-hydrogen microwave plasmas by heat loss calorimetry [32]. No increase in temperature with the addition of hydrogen to xenon was observed. In contrast, a remarkable temperature increase was observed when hydrogen was added to the helium microwave plasma. The temperature rise as a function of time for helium alone and the helium-hydrogen mixture (90/10%) is shown in Figure 8. The microwave input power to the helium alone was set at 60 W, and the input power to the helium-hydrogen mixture was 30 W. In both cases, the constant microwave input was maintained for 90 seconds and then terminated. The cooling curves were then recorded.

A conservative measure of the total output power was determined by taking the ratio of the areas of the helium-hydrogen temperature-rise-above-ambient-versus-time curve compared to that of helium only normalized by the ratio of the input powers. The ratio of the areas was determined to be about a factor of 10. The reactor volume was $10\,cm^3$ and the hydrogen flow rate was 1 sccm. Thus, with a microwave input power

of 30 $W$, the thermal output power was measured to be at least 300 $W$ corresponding to a reactor temperature rise from room temperature to 900 °C within 90 seconds, a power density of over 30 $MW/m^3$, and an energy balance of over $-4 X 10^5$ $kJ/mole\ H_2$ compared to the enthalpy of combustion of hydrogen of $-241.8$ $kJ/mole\ H_2$.

A more accurate measure was determined by modeling the heat flow from the quartz reactor wherein the parameters of the model were taken from the Newton cooling curves. Consider a small heat increment

$$dQ_t = P_{out}dt = dQ_m + dQ_l = CdT_h - CdT_c \tag{11}$$

where $Q_t$ is the total heat, $Q_m$ is the measured heat, $Q_l$ is the lost heat, $P_{out}$ is the power output, $t$ is time, $C$ is the system heat capacity, $dT_h$ is the temperature rise due to heating, and $dT_c$ is the temperature drop due to cooling ($dT_c$ is negative). The system heat capacity is a function of temperature, and at a given temperature, the power output can be expressed by the following equation,

$$P_{out} = C\left(\frac{dT_h}{dt} - \frac{dT_c}{dt}\right) \tag{12}$$

The slopes $dT_h/dt$ and $dT_c/dt$ can be calculated from the heating and cooling curves, respectively. Assuming that, at a given temperature, the heat capacities of the two systems (system 1: helium alone; system 2: helium-hydrogen) are the same, $C_1 = C_2$, then the power ratio can be calculated by

$$R = \frac{P_{out,2}}{P_{out,1}} = \frac{\left(\frac{dT_{h,2}}{dt} - \frac{dT_{c,2}}{dt}\right)}{\left(\frac{dT_{h,1}}{dt} - \frac{dT_{c,1}}{dt}\right)} \tag{13}$$

The slopes of the heating and cooling curves were calculated using the experimental data presented in Figure 8. The power ratios were calculated by Eq. (13) in the temperature range $\Delta T = 50 - 150\ °C$, where $\Delta T$ was the difference between the plasma temperature and the room temperature, 24 °C. The calculated results are given in Table 2. The average power ratio is $R = 5.35$ with a standard deviation of 0.23. The following power balance existed in the microwave plasma systems,

$$P_{out} = P_{in} + P_{ex} \tag{14}$$

where $P_{in}$ was the input power and $P_{ex}$ was the excess power. For the helium plasma, there was no excess power, $P_{ex,1} = 0$, $P_{out,1} = P_{in,1} = 60\ W$.

Therefore, at microwave input power of $30\,W$, the thermal output power was measured to be $P_{out.\,2} = 321 \pm 14\,W$ corresponding to an excess power of $291 \pm 14\,W$ and an unoptimized gain of about 11 times the input power.

## IV. CONCLUSION

We report that extreme ultraviolet (EUV) spectroscopy was recorded on microwave and glow discharges of helium with 2% hydrogen. Novel emission lines were observed with energies of $q \cdot 13.6\,eV$ where $q = 1,2,3,4,6,7,8,9,$ *or* 11 or these lines inelastically scattered by helium atoms wherein $21.2\,eV$ was absorbed in the excitation of $He\,(1s^2)$ to $He\,(1s^1 2p^1)$. These lines were identified as hydrogen transitions to electronic energy levels below the "ground" state corresponding to fractional quantum numbers. In glow discharge plasmas, an average hydrogen atom temperature of 33-38 $eV$ was observed by line broadening with the presence of helium ion catalyst with hydrogen; whereas, pure hydrogen plasmas showed no excessive broadening corresponding to an average hydrogen atom temperature of $\approx 3\,eV$.

Excess thermal power of about $300\,W$ and a gain of over an order of magnitude was observed from helium-hydrogen microwave plasmas. The power from the catalytic reaction of helium ions with atomic hydrogen corresponded to a volumetric power density of over $30\,MW/m^3$ which is about 100 times that of many coal fired electric power plants, and rivals some internal combustion engines. In addition, the presently observed and previously reported energy balances [13-14] were over $100\,eV/H\,atom$ which matched the present and previously reported EUV emission that corresponded to over $100\,eV/H\,atom$ [7-9, 17]. Since the net enthalpy released is at least 100 times that of combustion, the catalysis of atomic hydrogen represents a new source of energy with $H_2O$ as the source of hydrogen fuel. Moreover, rather that air pollutants or radioactive waste, novel hydride compounds with potential commercial applications are the products [20-26]. Since the power is in the form of a plasma that may form at room temperature, high-efficiency, low cost direct energy conversion may be possible, thus, avoiding heat engines such as turbines and the severe limitations of fuel cells [27-28]. Significantly lower capital costs and lower commercial operating costs

than that of any known competing energy source are anticipated.

## ACKNOWLEDGMENT

Special thanks to Y. Lu and T. Onuma for recording some spectra.

## REFERENCES

1. R. Mills, *The Grand Unified Theory of Classical Quantum Mechanics*, January 2000 Edition, BlackLight Power, Inc., Cranbury, New Jersey, Distributed by Amazon.com; posted at www.blacklightpower.com.
2. R. Mills, "The Grand Unified Theory of Classical Quantum Mechanics", Global Foundation, Inc. Orbis Scientiae entitled *The Role of Attractive and Repulsive Gravitational Forces in Cosmic Acceleration of Particles The Origin of the Cosmic Gamma Ray Bursts*, (29th Conference on High Energy Physics and Cosmology Since 1964) Dr. Behram N. Kursunoglu, Chairman, December 14-17, 2000, Lago Mar Resort, Fort Lauderdale, FL.
3. R. Mills, "The Grand Unified Theory of Classical Quantum Mechanics", Global Foundation, Inc. Orbis Scientiae entitled *The Role of Attractive and Repulsive Gravitational Forces in Cosmic Acceleration of Particles The Origin of the Cosmic Gamma Ray Bursts*, (29th Conference on High Energy Physics and Cosmology Since 1964) Dr. Behram N. Kursunoglu, Chairman, December 14-17, 2000, Lago Mar Resort, Fort Lauderdale, FL, Kluwer Academic/Plenum Publishers, New York, pp. 243-258.
4. R. Mills, "The Grand Unified Theory of Classical Quantum Mechanics", Int. J. of Hydrogen Energy, in press.
5. R. Mills, "The Hydrogen Atom Revisited", Int. J. of Hydrogen Energy, Vol. 25, Issue 12, December, (2000), pp. 1171-1183.
6. R. Mills, The Nature of Free Electrons in Superfluid Helium--a Test of Quantum Mechanics and a Basis to Review its Foundations and Make a Comparison to Classical Theory, Int. J. Hydrogen Energy, Vol. 26, No. 10, (2001), pp. 1059-1096.
7. R. Mills, P. Ray, "Spectral Emission of Fractional Quantum Energy Levels of Atomic Hydrogen from a Helium-Hydrogen Plasma and the Implications for Dark Matter", Int. J. Hydrogen Energy, in press.

8. R. Mills, P. Ray, "Vibrational Spectral Emission of Fractional-Principal-Quantum-Energy-Level Hydrogen Molecular Ion", Int. J. Hydrogen Energy, in press.
9. R. Mills, P. Ray, Spectroscopic Identification of a Novel Catalytic Reaction of Potassium and Atomic Hydrogen and the Hydride Ion Product, Int. J. Hydrogen Energy, in press.
10. R. Mills, "Spectroscopic Identification of a Novel Catalytic Reaction of Atomic Hydrogen and the Hydride Ion Product", Int. J. Hydrogen Energy, Vol. 26, No. 10, (2001), pp. 1041-1058.
11. R. Mills and M. Nansteel, "Argon-Hydrogen-Strontium Plasma Light Source", IEEE Transactions on Plasma Science, submitted.
12. R. Mills, M. Nansteel, and Y. Lu, "Excessively Bright Hydrogen-Strontium Plasma Light Source Due to Energy Resonance of Strontium with Hydrogen", European Journal of Physics D, submitted.
13. R. Mills, A. Voigt, P. Ray, M. Nanstell, "Measurement of Hydrogen Balmer Line Broadening and Thermal Power Balances of Noble Gas-Hydrogen Discharge Plasmas", Int. J. Hydrogen Energy, submitted.
14. R. Mills, N. Greenig, S. Hicks, "Optically Measured Power Balances of Anomalous Discharges of Mixtures of Argon, Hydrogen, and Potassium, Rubidium, Cesium, or Strontium Vapor", Int. J. Hydrogen Energy, submitted.
15. R. Mills, M. Nansteel, and Y. Lu, "Observation of Extreme Ultraviolet Hydrogen Emission from Incandescently Heated Hydrogen Gas with Strontium that Produced an Anomalous Optically Measured Power Balance", Int. J. Hydrogen Energy, Vol. 26, No. 4, (2001), pp. 309-326.
16. R. Mills, J. Dong, Y. Lu, "Observation of Extreme Ultraviolet Hydrogen Emission from Incandescently Heated Hydrogen Gas with Certain Catalysts", Int. J. Hydrogen Energy, Vol. 25, (2000), pp. 919-943.
17. R. Mills, "Observation of Extreme Ultraviolet Emission from Hydrogen-KI Plasmas Produced by a Hollow Cathode Discharge", Int. J. Hydrogen Energy, Vol. 26, No. 6, (2001), pp. 579-592.
18. R. Mills, "Temporal Behavior of Light-Emission in the Visible Spectral Range from a Ti-K2CO3-H-Cell", Int. J. Hydrogen Energy, Vol. 26, No. 4, (2001), pp. 327-332.
19. R. Mills, T. Onuma, and Y. Lu, "Formation of a Hydrogen Plasma from an Incandescently Heated Hydrogen-Catalyst Gas Mixture with an

Anomalous Afterglow Duration", Int. J. Hydrogen Energy, Vol. 26, No. 7, July, (2001), pp. 749-762.

20. R. Mills, B. Dhandapani, M. Nansteel, J. He, A. Voigt, "Identification of Compounds Containing Novel Hydride Ions by Nuclear Magnetic Resonance Spectroscopy", Int. J. Hydrogen Energy, Vol. 26, No. 9, Sept. (2001), pp. 965-979.
21. R. Mills, B. Dhandapani, N. Greenig, J. He, "Synthesis and Characterization of Potassium Iodo Hydride", Int. J. of Hydrogen Energy, Vol. 25, Issue 12, December, (2000), pp. 1185-1203.
22. R. Mills, "Novel Inorganic Hydride", Int. J. of Hydrogen Energy, Vol. 25, (2000), pp. 669-683.
23. R. Mills, "Novel Hydrogen Compounds from a Potassium Carbonate Electrolytic Cell", Fusion Technology, Vol. 37, No. 2, March, (2000), pp. 157-182.
24. R. Mills, B. Dhandapani, M. Nansteel, J. He, T. Shannon, A. Echezuria, "Synthesis and Characterization of Novel Hydride Compounds", Int. J. of Hydrogen Energy, Vol. 26, No. 4, (2001), pp. 339-367.
25. R. Mills, "Highly Stable Novel Inorganic Hydrides", Journal of Materials Research, submitted.
26. R. Mills, W. Good, A. Voigt, Jinquan Dong, "Minimum Heat of Formation of Potassium Iodo Hydride", Int. J. Hydrogen Energy, Vol. 26, No. 11, Oct., (2001), pp. 1199-1208.
27. R. Mills, "BlackLight Power Technology-A New Clean Hydrogen Energy Source with the Potential for Direct Conversion to Electricity", Proceedings of the National Hydrogen Association, 12 th Annual U.S. Hydrogen Meeting and Exposition, *Hydrogen: The Common Thread*, The Washington Hilton and Towers, Washington DC, (March 6-8, 2001), pp. 671-697.
28. R. Mills, "BlackLight Power Technology-A New Clean Energy Source with the Potential for Direct Conversion to Electricity", Global Foundation International Conference on "Global Warming and Energy Policy", Dr. Behram N. Kursunoglu, Chairman, Fort Lauderdale, FL, November 26-28, 2000, Kluwer Academic/Plenum Publishers, New York, pp. 1059-1096.
29. B. J. Thompson, Handbook of Nonlinear Optics, Marcel Dekker, Inc., New York, (1996), pp. 497-548.

30. Y. R. Shen, The Principles of Nonlinear Optics, John Wiley & Sons, New York, (1984), pp. 203-210.
31. B. de Beauvoir, F. Nez, L. Julien, B. Cagnac, F. Biraben, D. Touahri, L. Hilico, O. Acef, A. Clairon, and J. J. Zondy, Physical Review Letters, Vol. 78, No. 3, (1997), pp. 440-443.
32. C. Chen, T. Wei, L. R. Collins, and J. Phillips, "Modeling the discharge region of a microwave generated hydrogen plasma", J. Phys. D: Appl. Phys., Vol. 32, (1999), pp. 688-698.
33. M. Kuraica, N. Konjevic, "Line shapes of atomic hydrogen in a plane-cathode abnormal glow discharge", Physical Review A, Volume 46, No. 7, October (1992), pp. 4429-4432.
34. I. R. Videnocíc, N. Konjevíc, M. M. Kuraica, "Spectroscopic investigations of a cathode fall region of the Grimm-type glow discharge", Spectrochimica Acta, Part B, Vol. 51, (1996), pp. 1707-1731.

Table 1. Observed line emission from helium-hydrogen plasmas assigned to the dominant disproportionation reactions given by Eqs. (4-7) and helium inelastic scattered peaks of hydrogen transitions, wherein the photon strikes $He\,(1s^2)$ and 21.2 $eV$ is absorbed in the excitation to $He\,(1s^1 2p^1)$.

| Observed Line (nm) | Predicted (Mills) (nm) | Assignment (Mills) | Figure # |
|---|---|---|---|
| 8.29 | 8.29 | $H\left[\frac{a_H}{3}\right] + H\left[\frac{a_H}{3}\right] \rightarrow H\left[\frac{a_H}{5}\right] + H\left[\frac{a_H}{2}\right] + 149.6\ eV$ | 3 |
| 10.13 | 10.13 | $H\left[\frac{a_H}{2}\right] + H\left[\frac{a_H}{2}\right] \rightarrow H\left[\frac{a_H}{4}\right] + H[a_H] + 122.4\ eV$ | 3 |
| 13.03[a] | 13.03 | $H\left[\frac{a_H}{3}\right] + H\left[\frac{a_H}{3}\right] \rightarrow H\left[\frac{a_H}{5}\right] + H^+ + e^- + 95.2\ eV$ | 3 |
| 14.15 | 14.15 | $H\left[\frac{a_H}{2}\right] + H\left[\frac{a_H}{2}\right] \rightarrow H\left[\frac{a_H}{4}\right] + H^+ + e^- + 108.8\ eV$<br>$108.8\ eV + He\,(1s^2) \rightarrow He\,(1s^1 2p^1) \rightarrow +87.59\ eV$ | 3 |
| 20.5 | 20.5 | $H\left[\frac{a_H}{4}\right] + H\left[\frac{a_H}{2}\right] \rightarrow H\left[\frac{a_H}{5}\right] + H[a_H] + 81.6\ eV$<br>$81.6\ eV + He\,(1s^2) \rightarrow He\,(1s^1 2p^1) \rightarrow +60.39\ eV$ | 2, 3 |
| 30.4 | 30.4 | $H\left[\frac{a_H}{3}\right] + H\left[\frac{a_H}{2}\right] \rightarrow H\left[\frac{a_H}{4}\right] + H^+ + e^- + 40.8\ eV$ | 2, 3 |
| 30.4 | 30.4 | $He^+(n=2) \rightarrow He^+(n=1) + 40.8\ eV$[b] | 2, 3 |
| 37.4 | 37.4 | $H[a_H] \xrightarrow{He^+} H\left[\frac{a_H}{3}\right] + 54.4\ eV + 54.4\ eV$<br>$54.4\ eV + He\,(1s^2) \rightarrow He\,(1s^1 2p^1) \rightarrow +33.19\ eV$ | 2, 3 |
| 45.6 | 45.6 | $H\left[\frac{a_H}{3}\right] + H\left[\frac{a_H}{3}\right] \rightarrow H\left[\frac{a_H}{4}\right] + H\left[\frac{a_H}{2}\right] + 27.2\ eV$ | 2, 3 |
| 58.4 | 58.4 | $He\,(1s^1 2p^1) \rightarrow He\,(1s^2) + 21.2\ eV$[c] | 4 |

| | | | |
|---|---|---|---|
| 63.3 | 63.3 | $H\left[\frac{a_H}{3}\right] + H\left[\frac{a_H}{2}\right] \rightarrow H\left[\frac{a_H}{4}\right] + H^+ + e^- + 40.8\ eV$<br>$40.8\ eV + He\ (1s^2) \rightarrow He\ (1s^1 2p^1) \rightarrow +19.59\ eV$ | 4 |
| 63.3 | 63.3 | $He^+(n=2) \rightarrow He^+(n=1) + 40.8\ eV$ [b]<br>$40.8\ eV + He\ (1s^2) \rightarrow He\ (1s^1 2p^1) \rightarrow +19.59\ eV$ | 4 |
| 91.2 | 91.2 | $H\left[\frac{a_H}{2}\right] + H\left[\frac{a_H}{2}\right] \rightarrow H\left[\frac{a_H}{3}\right] + H^+ + e^- + 13.6\ eV$ | 5 |
| 91.2 | 91.2 | $H^+ + e^- \rightarrow H[a_H] + 13.6\ eV$ [d] | 6 |

[a] Weak shoulder on the 14.15 nm peak.

[b] In Figures 2 and 3, the peak corresponding to $He^+(n=3) \rightarrow He^+(n=1) + 48.35\ eV$ ($25.6\ nm$)was absent which makes this assignment difficult.

[c] The intensity was 56,771 photons/sec in Figure 4; thus, the transition $He\ (1s^2) \rightarrow He\ (1s^1 2p^1)$ dominated the inelastic scattering of EUV peaks.

[d] The ratio of the L$\beta$ peak to the 91.2 nm peak of the helium-hydrogen plasma shown in Figure 5 was 2; whereas, the ratio of the L$\beta$ peak to the 91.2 nm peak of the control hydrogen plasma shown in Figure 6, was 8 which makes this assignment difficult.

Table 2. Calculation of Power Ratios between Helium-Hydrogen and Helium Plasmas.

| $\Delta T$ (°C) | $dT_{h,1}/dt$ (°C/sec) | $dT_{c,1}/dt$ (°C/sec) | $dT_{h,2}/dt$ (°C/sec) | $dT_{c,2}/dt$ (°C/sec) | Power Ratio, $R$ |
|---|---|---|---|---|---|
| 50 | 10.731 | -0.800 | 55.951 | -0.989 | 4.938 |
| 60 | 9.801 | -1.004 | 54.893 | -1.118 | 5.183 |
| 70 | 9.020 | -1.255 | 53.874 | -1.266 | 5.367 |
| 80 | 8.354 | -1.549 | 52.892 | -1.433 | 5.486 |
| 90 | 7.779 | -1.876 | 51.946 | -1.619 | 5.548 |
| 100 | 7.279 | -2.216 | 51.032 | -1.819 | 5.566 |
| 110 | 6.839 | -2.551 | 50.150 | -2.025 | 5.557 |
| 120 | 6.449 | -2.879 | 49.299 | -2.222 | 5.523 |
| 130 | 6.101 | -3.235 | 48.475 | -2.390 | 5.448 |
| 140 | 5.789 | -3.716 | 47.679 | -2.507 | 5.280 |
| 150 | 5.507 | -4.561 | 46.908 | -2.555 | 4.913 |

## Figure Captions

Figure 1. The experimental set up comprising a microwave discharge gas cell light source and an EUV spectrometer which was differentially pumped.

Figure 2. The EUV spectra ($15-50\,nm$) of the microwave cell emission of the helium-hydrogen mixture (98/2%) recorded at 1, 24, and 72 hours with a normal incidence EUV spectrometer and a CEM, and control helium (dotted curve) recorded with a 4° grazing incidence EUV spectrometer and a CEM. The pressure was maintained at 20 torr. Only known He I and He II peaks were observed with the helium control. Reproducible novel emission lines that increased with time were observed at $45.6\,nm$ and $30.4\,nm$ with energies of $q \cdot 13.6\,eV$ where $q = 2\ or\ 3$ and at $37.4\,nm$ and $20.5\,nm$ with energies of $q \cdot 13.6\,eV$ where $q = 4\ or\ 6$ that were inelastically scattered by helium atoms wherein $21.2\,eV$ ($58.4\,nm$) was absorbed in the excitation of $He(1s^2)$. These lines were identified in Table 1 as hydrogen transitions to electronic energy levels below the "ground" state corresponding to fractional quantum numbers.

Figure 3. The short wavelength EUV spectra ($5-50\,nm$) of the microwave cell emission of the helium-hydrogen mixture (98/2%) (top curve) and control hydrogen (bottom curve) recorded with a normal incidence EUV spectrometer and a CEM. No hydrogen emission was observed in this region, and no instrument artifacts were observed. Reproducible novel emission lines were observed at $45.6\,nm$, $30.4\,nm$, $13.03\,nm$, $10.13\,nm$, and $8.29\,nm$ with energies of $q \cdot 13.6\,eV$ where $q = 2,3,7,9,\ or\ 11$ and at $37.4\,nm$, $20.5\,nm$, and $14.15\,nm$ with energies of $q \cdot 13.6\,eV$ where $q = 4,6,\ or\ 8$ that were inelastically scattered by helium atoms wherein $21.2\,eV$ ($58.4\,nm$) was absorbed in the excitation of $He(1s^2)$. These lines were identified in Table 1 as hydrogen transitions to electronic energy levels below the "ground" state corresponding to fractional quantum numbers.

Figure 4. The EUV spectrum ($50-65\,nm$) of the helium-hydrogen mixture (98/2%) glow discharge cell emission recorded with a 4° grazing incidence EUV spectrometer and a CEM. The pressure was maintained at 400 mtorr. A novel line was observed at $63.3\,nm$ corresponding to the $30.4\,nm$ lower-energy hydrogen transition line shown in Figures 2 and 3

and Table 1 that was inelastically scattered by helium atoms wherein $21.2\,eV$ ($58.4\,nm$) was absorbed in the excitation of $He(1s^2)$.

Figure 5. The EUV spectrum ($88-125\,nm$) of the helium-hydrogen mixture (98/2%) microwave cell emission recorded with a normal incidence EUV spectrometer and a CEM. The pressure was maintained at 20 torr. An emission line was observed at $91.2\,nm$ with an energy of $q \cdot 13.6\,eV$ where $q=1$ which was identified in Table 1 as hydrogen transitions to electronic energy levels below the "ground" state corresponding to fractional quantum numbers based on the $91.2\,nm$ line intensity relative to $L\beta$ compared to that of the control hydrogen plasma.

Figure 6. The EUV spectrum ($80-105\,nm$) of the control hydrogen microwave discharge cell emission recorded with a normal incidence EUV spectrometer and a CEM.

Figure 7. The 656.2 nm Balmer $\alpha$ line width recorded with a high resolution ($\pm 0.025\,nm$) visible spectrometer on a helium-hydrogen mixture (90/10%) discharge plasma. Significant broadening was observed corresponding to an average hydrogen atom temperature of $33-38\,eV$.

Figure 8. The temperature rise as a function of time for helium alone and the helium-hydrogen mixture (90/10%) with microwave input power set at 60 W and 30 W, respectively. In both cases, the constant microwave input was maintained for 90 seconds and then terminated. The cooling curves were then recorded. The maximum $\Delta T$ for helium-hydrogen mixture and helium alone was 873 °C and 178 °C, respectively. The thermal output power of the helium-hydrogen plasma was determined to be at least $300\,W$.

Fig. 1

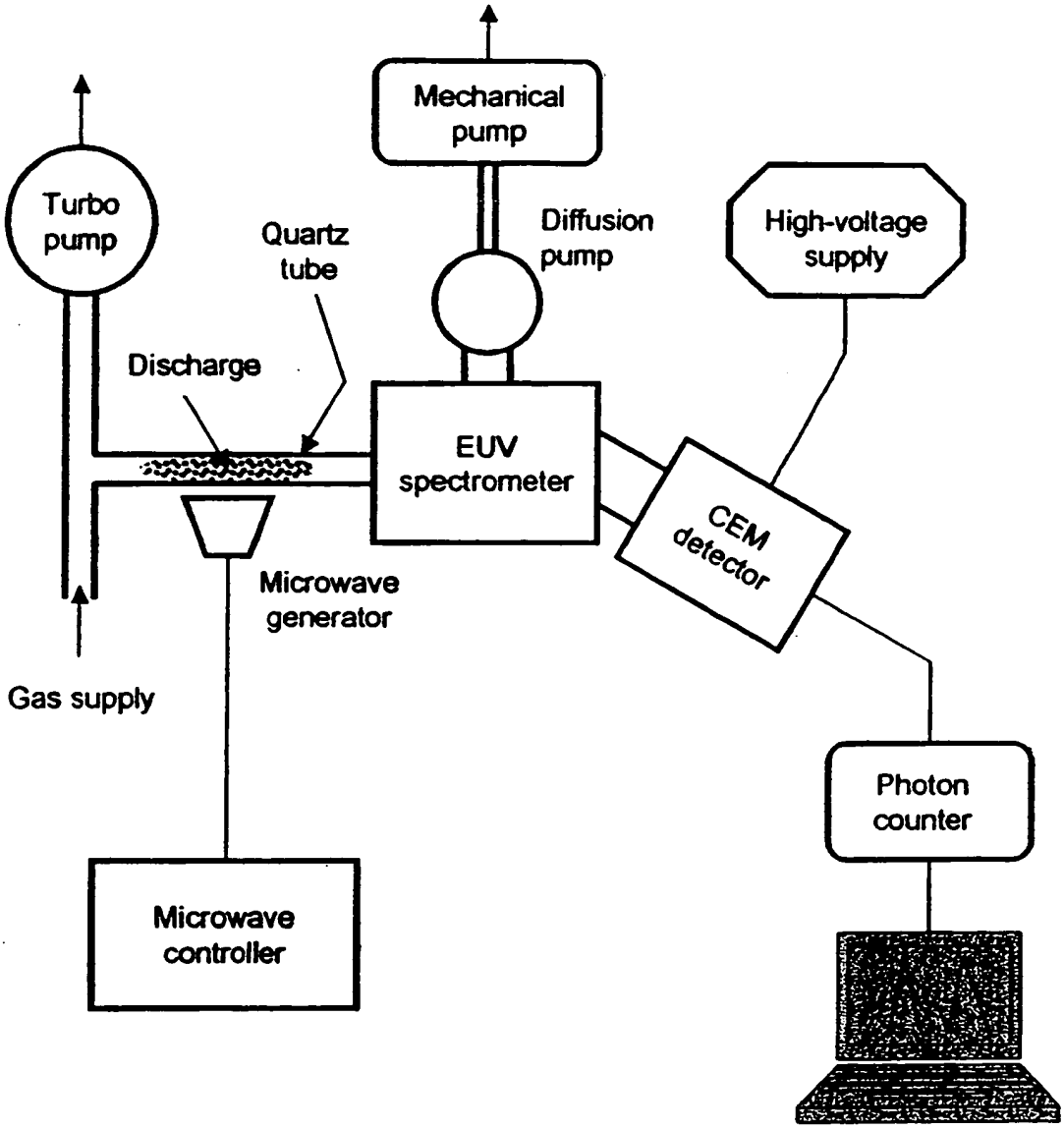
Mechanical pump
Turbo pump
Quartz tube
Diffusion pump
High-voltage supply
Discharge
EUV spectrometer
CEM detector
Microwave generator
Gas supply
Photon counter
Microwave controller

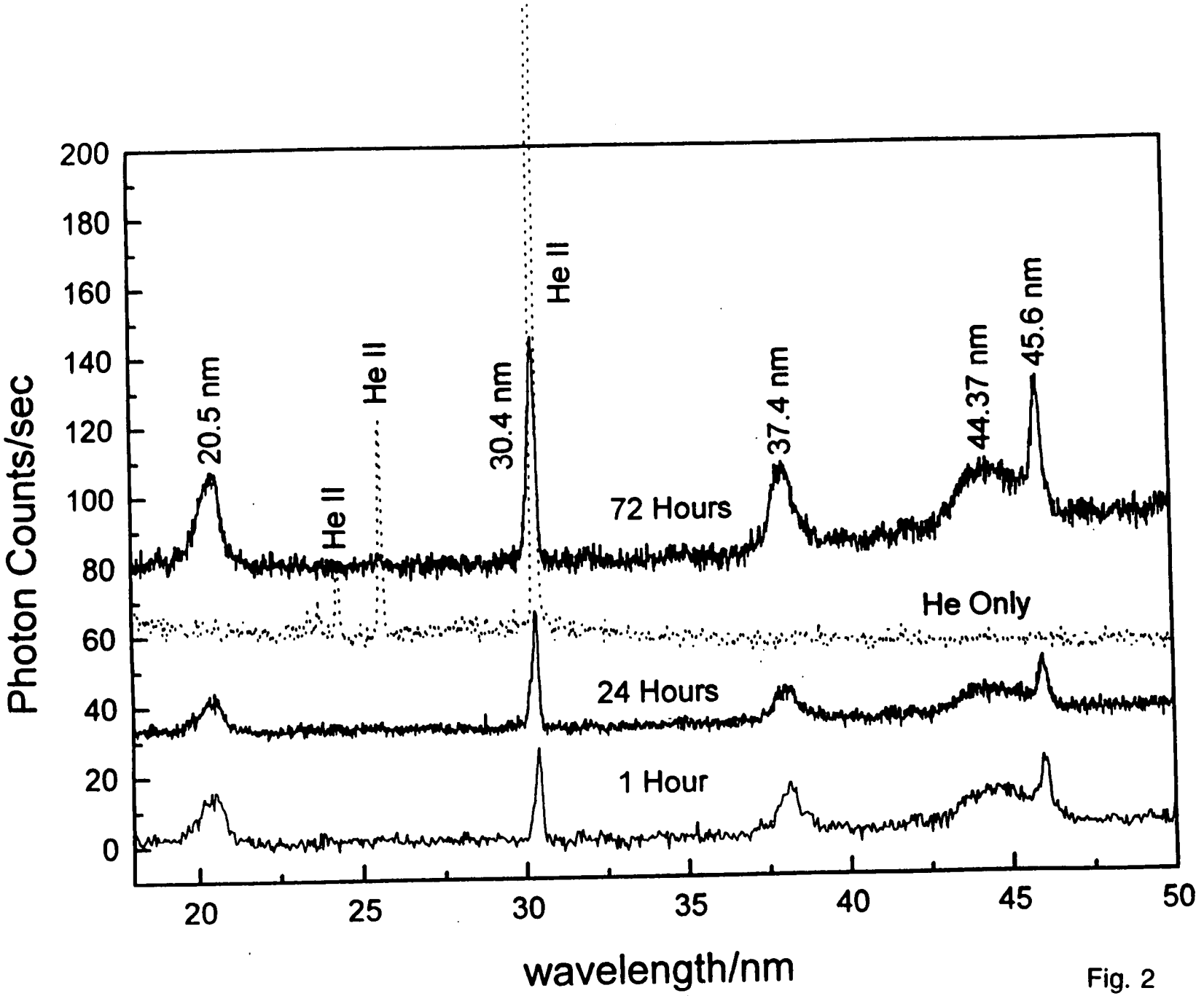
Photon Counts/sec
200
180
160
140
120
100
80
60
40
20
0
20.5 nm
He II
He II
30.4 nm
He II
37.4 nm
44.37 nm
45.6 nm
72 Hours
He Only
24 Hours
1 Hour
20
25
30
35
40
45
50
wavelength/nm

Fig. 2

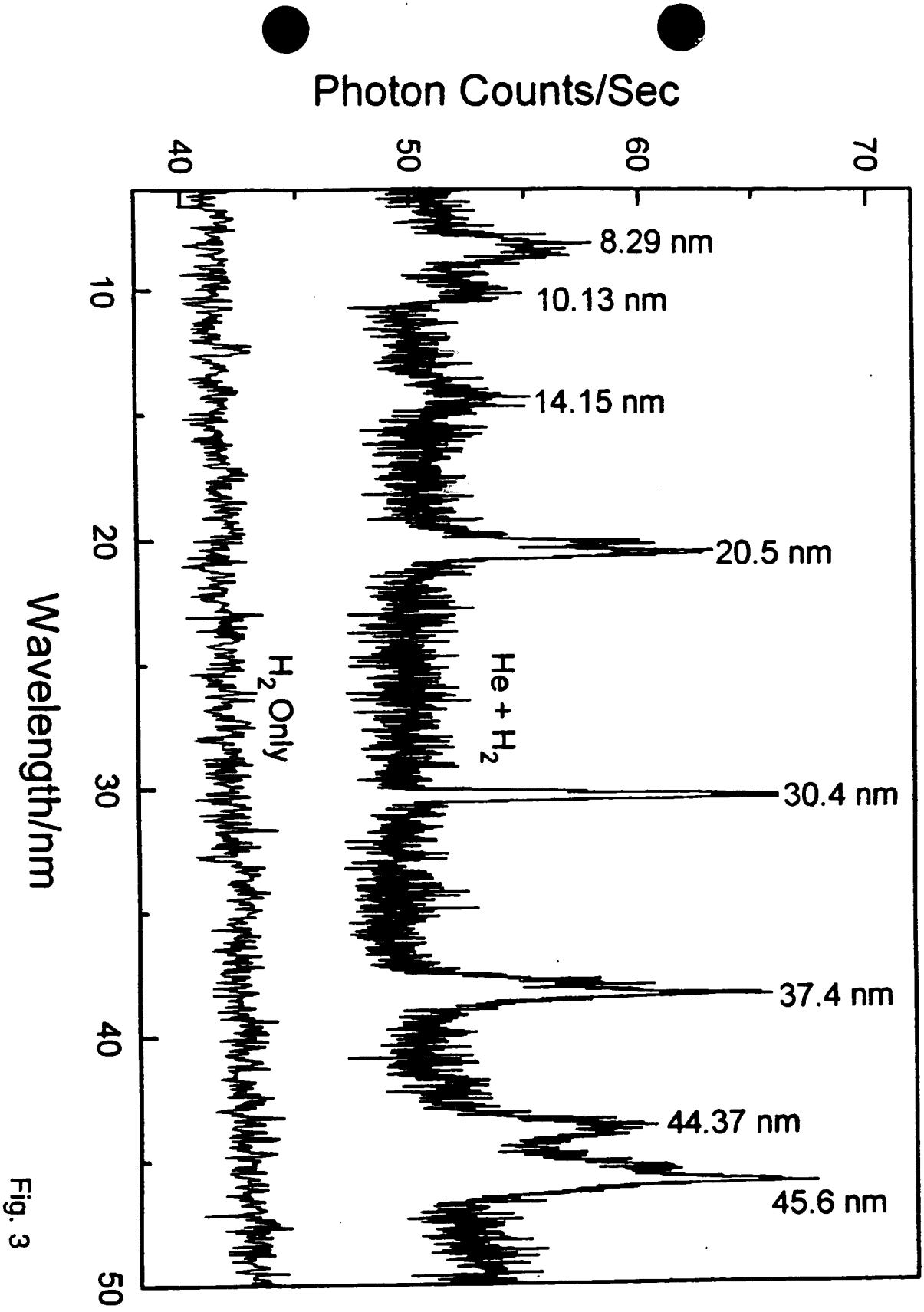
Photon Counts/Sec
40
50
60
70
Wavelength/nm
10
20
30
40
50
8.29 nm
10.13 nm
14.15 nm
20.5 nm
30.4 nm
37.4 nm
44.37 nm
45.6 nm
H2 Only
He + H2

Fig. 3

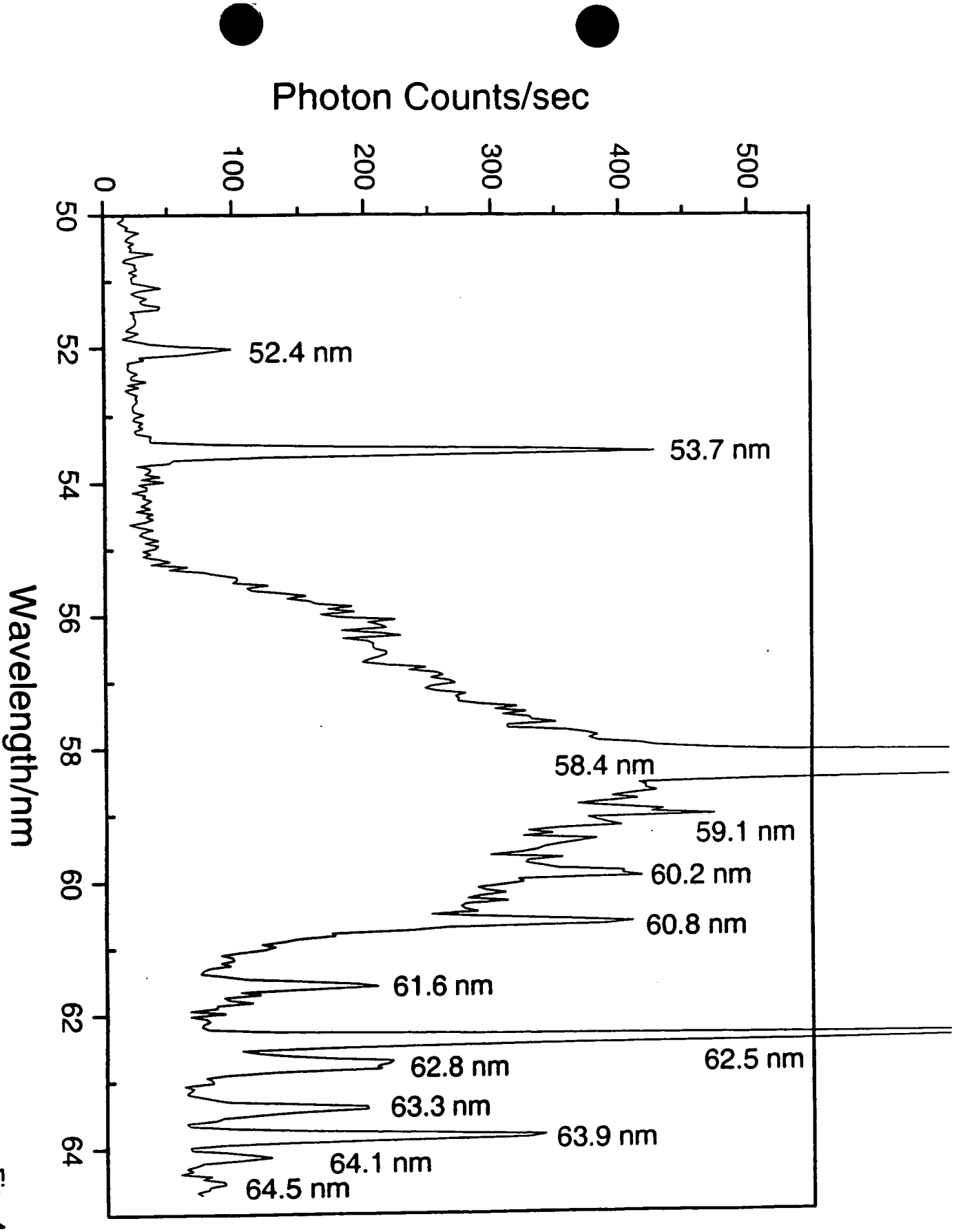
Photon Counts/sec
0
100
200
300
400
500
Wavelength/nm
50
52
54
56
58
60
62
64
52.4 nm
53.7 nm
58.4 nm
59.1 nm
60.2 nm
60.8 nm
61.6 nm
62.5 nm
62.8 nm
63.3 nm
63.9 nm
64.1 nm
64.5 nm

Fig. 4

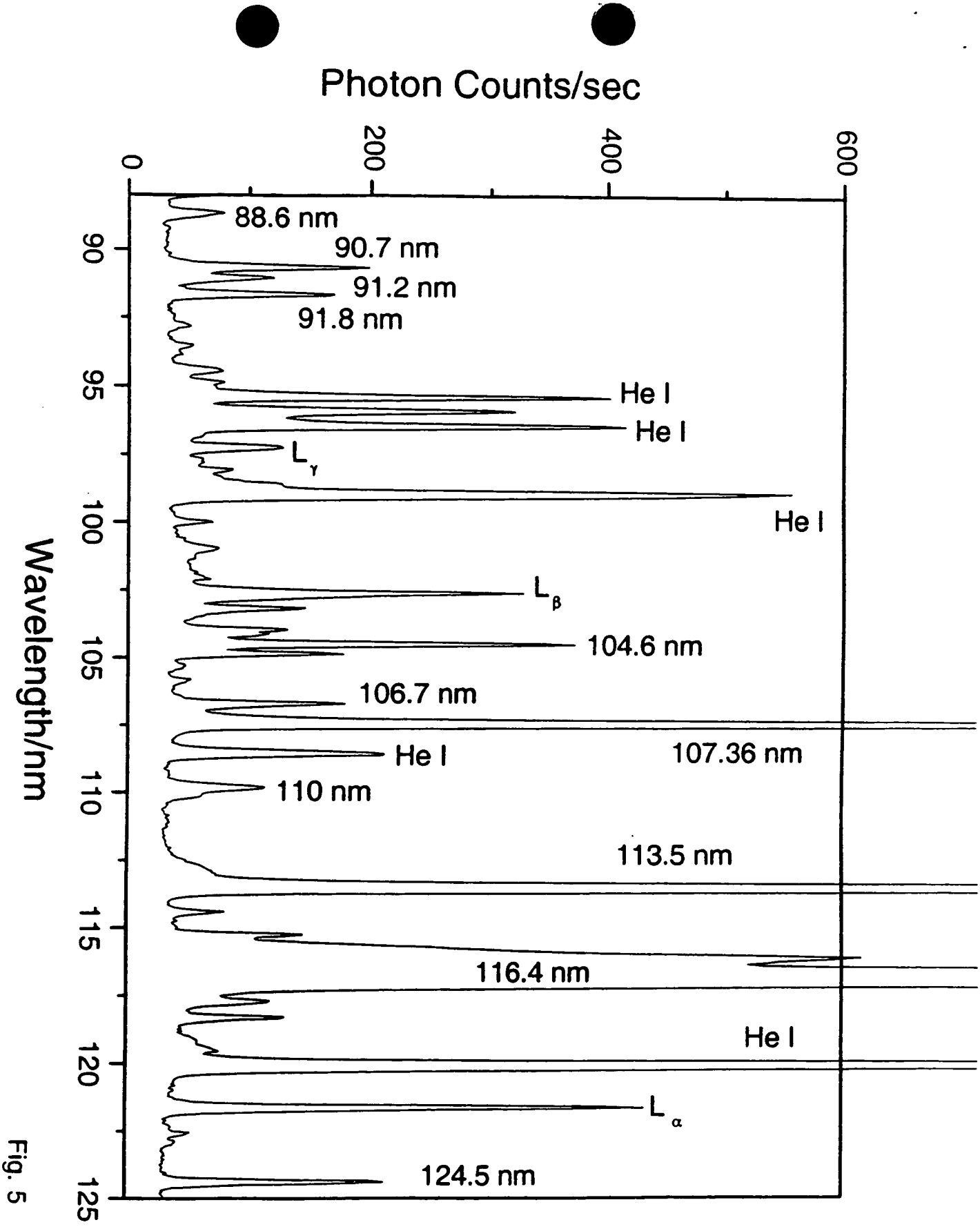
Photon Counts/sec
0
200
400
600
Wavelength/nm
90
95
100
105
110
115
120
125
88.6 nm
90.7 nm
91.2 nm
91.8 nm
He I
He I
$L_\gamma$
He I
$L_\beta$
104.6 nm
106.7 nm
He I
107.36 nm
110 nm
113.5 nm
116.4 nm
He I
$L_\alpha$
124.5 nm

Fig. 5

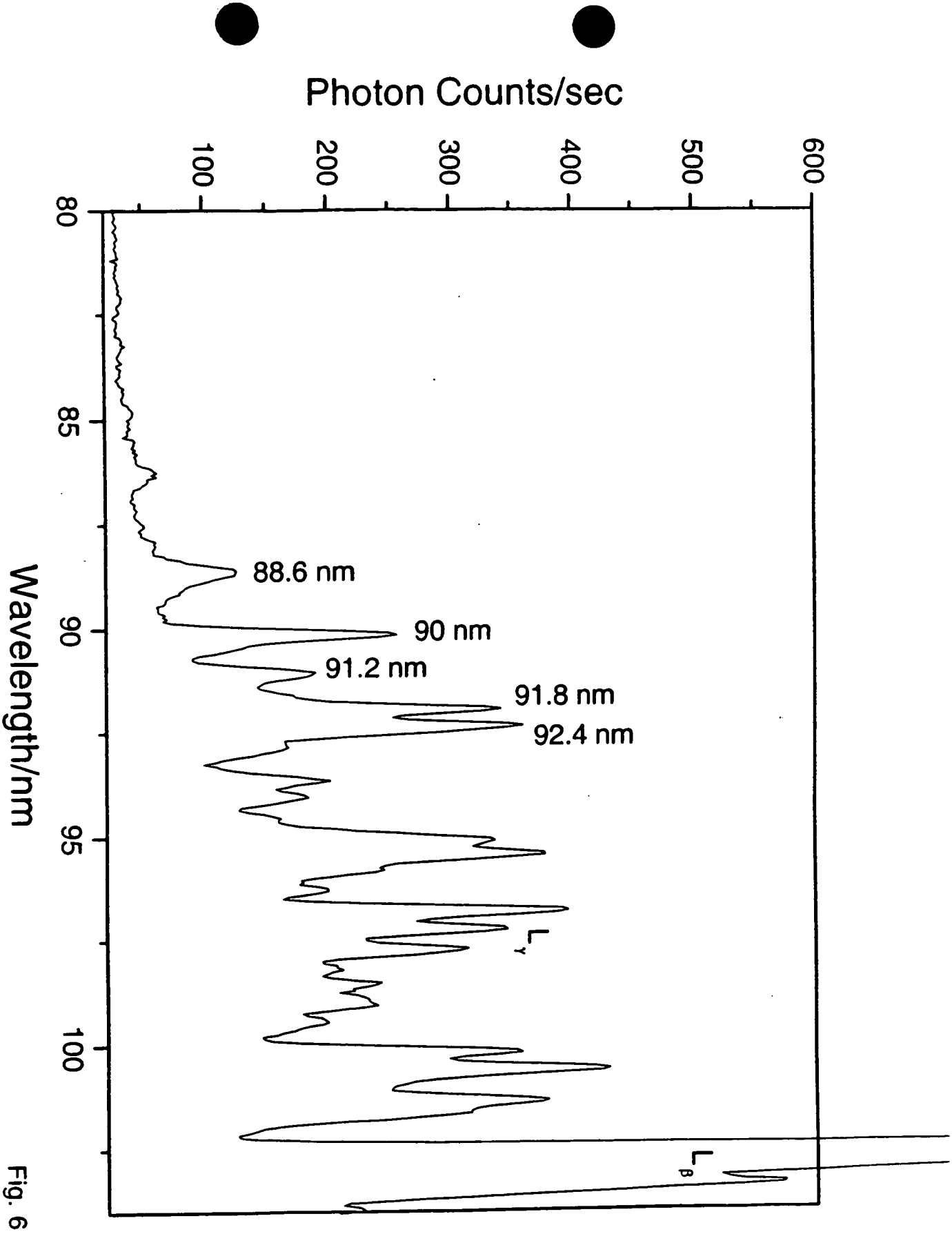
Photon Counts/sec
100
200
300
400
500
600
Wavelength/nm
80
85
90
95
100
88.6 nm
90 nm
91.2 nm
91.8 nm
92.4 nm
$L_\gamma$
$L_\beta$

Fig. 6

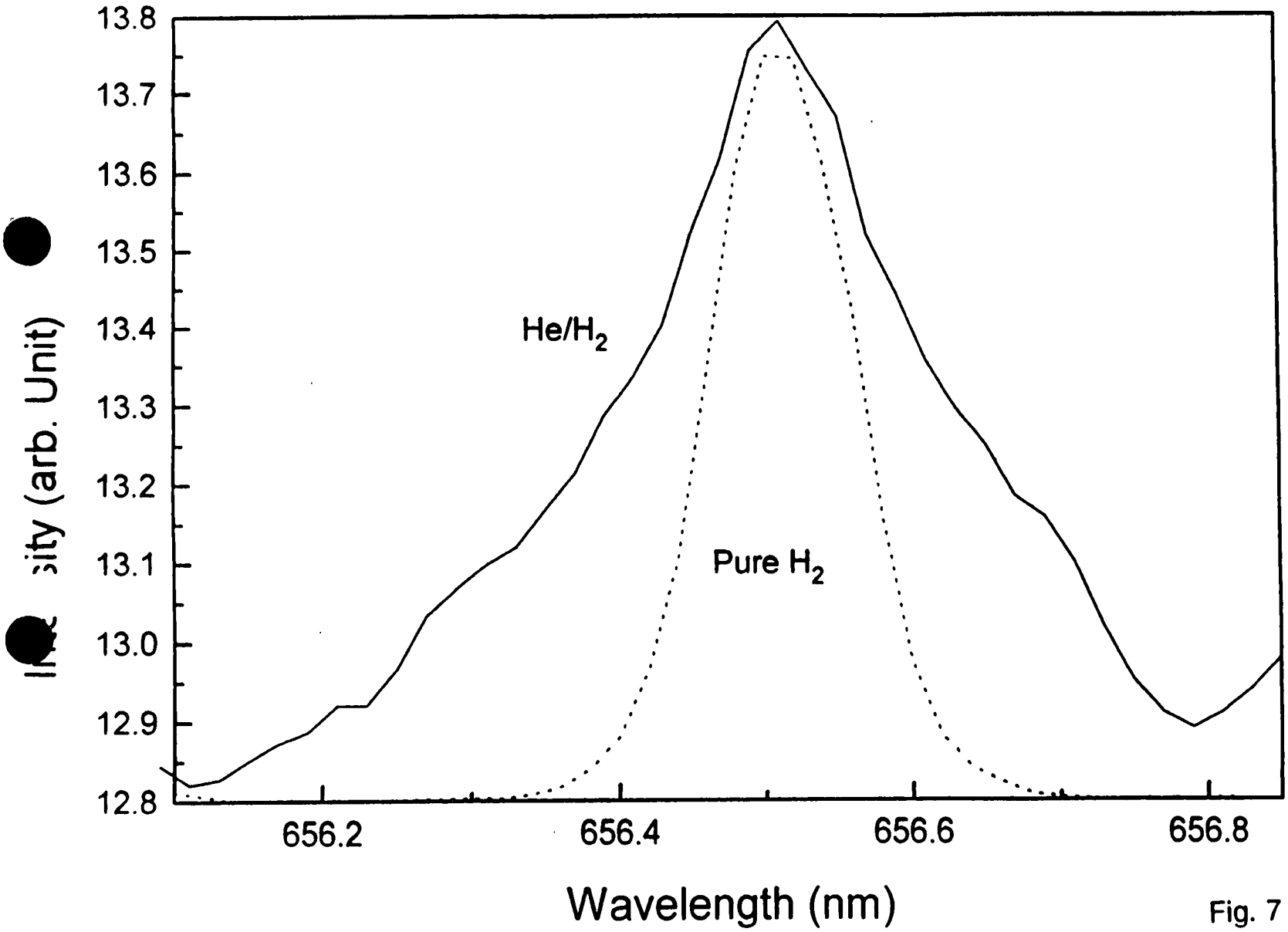
13.8
13.7
13.6
13.5
13.4
13.3
13.2
13.1
13.0
12.9
12.8
He/H2
Pure H2
656.2
656.4
656.6
656.8
Wavelength (nm)

Fig. 7

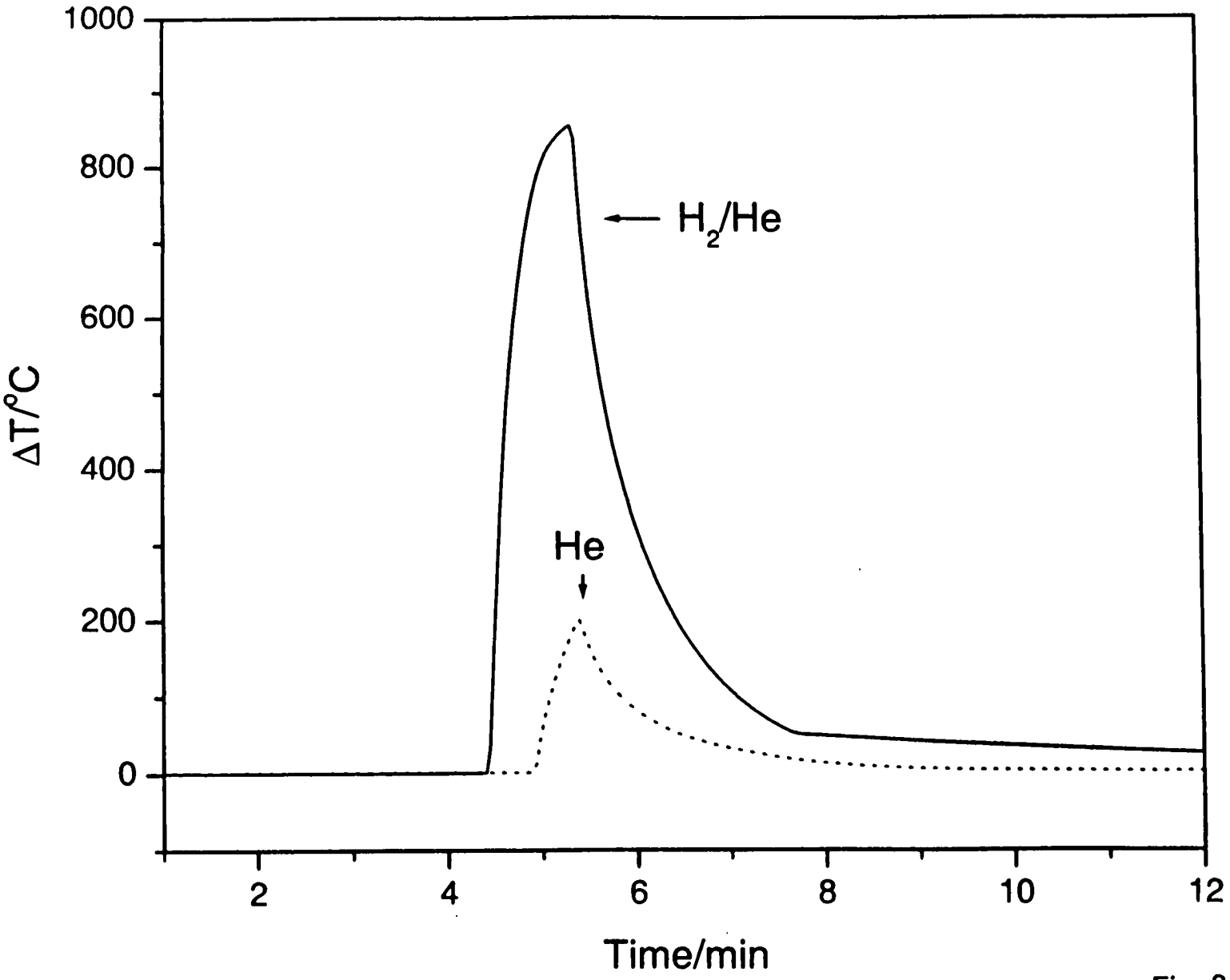


Fig. 8